

Conditions for defect-free solidification of aqueous ammonium chloride in a quasi two-dimensional directional solidification facility

S.H. Whiteoak*, Herbert E. Huppert, M. Grae Worster

Institute of Theoretical Geophysics, Department of Applied Mathematics and Theoretical Physics, University of Cambridge, Wilberforce Road, Cambridge CB3 0WA, UK

ARTICLE INFO

Article history:

Received 8 February 2008

Received in revised form

24 April 2008

Accepted 28 April 2008

Communicated by M. Rettenmayr

Available online 8 May 2008

PACS:

64.70.-p

Keywords:

A1. Directional solidification

B1. Chimneys

B1. Mushy layer

ABSTRACT

Experimental and theoretical approaches to the problem of the solidification of a binary melt are presented. We describe a series of experiments in which aqueous solutions of ammonium chloride of above eutectic composition are cooled from below in a Hele–Shaw cell that is translated downwards at a constant rate. A mushy layer of solid dendrites bathed in a salt-depleted interstitial fluid is formed. For certain combinations of initial concentration and translation speed, convection in the mush gives rise to chimneys which result in defects in the solidified material. Our experiments demonstrate that using a higher temperature gradient for solidification increases the range of conditions for which a mushy layer forms that is free from both chimneys and secondary nucleation. We present a mathematical model of the system, to which we derive an approximate analytical solution. Predictions of the height of the mushy layer given by this approximate solution are found to be in excellent agreement with full numerical predictions when the height is small. Both numerical and analytical predictions are a better match to experimental data when the temperature gradient is low.

© 2008 Elsevier B.V. All rights reserved.

1. Introduction

Directional solidification, in which a melt is cooled and solidified by pulling it through a constant temperature gradient, is a method of casting a metallic alloy that is used in the manufacture of many different industrial products. The manufacture of turbine blades is a typical example, the aim being to form a blade that is free from grain boundaries and therefore resistant to creep [1]. During the directional solidification of a binary melt, the interface between solid and liquid generally becomes morphologically unstable, resulting in a mushy layer of solid dendrites bathed in interstitial fluid. In the case of a melt which, upon solidification, releases fluid of a lower density than the original solution, cooling from below causes two modes of convection to be set up: a boundary layer mode and a mushy layer mode [2,3].

Upflow of interstitial fluid due to convection in the mushy layer creates regions of low solid fraction. Owing to pieces of dendrite being dissolved by the convected fluid, the porosity of these regions is increased and thus convection is even further encouraged here, until eventually almost all upflow occurs through narrow, dendrite-free channels known as chimneys. In

terms of $\Delta C = C_0 - C_E$, where C_0 is the initial concentration of the melt and C_E is the eutectic composition, the strength of convection in the mush is governed by a Rayleigh number

$$R_m = \frac{\beta \Delta C g \Pi_0 h}{\kappa \nu}, \quad (1)$$

where h is the height of the mushy layer, Π_0 is a representative value of the permeability and β , κ and ν are, respectively, the solutal density coefficient, the thermal diffusivity and the kinematic viscosity of the melt. In particular, convection occurs only when this number is greater than some critical value [2,4].

Chimneys formed during directional solidification lead to defects in the metal (freckles) which undesirably decrease its strength. A great deal of research has been carried out with the aim of understanding the conditions under which chimneys form. Extensive use has been made of aqueous ammonium chloride solutions [5–7] because the phase diagram and microstructure mimic that of the metallic alloys used in turbine blade manufacture, they are far easier to work with in the laboratory and they are transparent, so that the structures formed during solidification can be seen. In Section 2 we describe how we utilise the experimental apparatus and procedure initially described in Ref. [8] to investigate the effect of different temperature gradients on the mode of solidification of aqueous ammonium chloride solutions. At each temperature gradient, our main focus is to determine the range of solidification conditions that will give a

* Corresponding author.

E-mail addresses: shw32@cam.ac.uk (S.H. Whiteoak), heh1@esc.cam.ac.uk (H.E. Huppert), grae@damtp.cam.ac.uk (M.G. Worster).

defect-free solid, and in Section 3 this information is clearly presented in a series of regime diagrams.

Directional solidification is modelled mathematically by considering the conservation of heat and solute in the melt and mushy layer. In Section 4 we present the governing equations and describe previous numerical solutions [9]. We include our own numerical predictions of the height of the mushy layer, and also derive an approximate analytical solution and use it to make predictions of h . Both sets of predictions are compared with experimental data. We present the conditions under which our approximate solution is valid in Appendix A.

Section 5 provides a discussion of the experimental and theoretical results. Section 6 summarises the main conclusions to be drawn from this work.

2. Experimental methods

Aqueous solutions of ammonium chloride, with concentrations ranging from 21% to 27% (by weight) were solidified in a Hele–Shaw cell of internal dimensions $38 \times 12 \times 0.5$ cm. A schematic of the experimental system is shown in Fig. 1(a). In each experiment, the cell was pulled at constant speed V between two heat exchangers, the lower of which was at a temperature below the eutectic temperature. Motion of the cell was achieved using a geared stepper motor which turned a screw driving the cell. The paper by Peppin et al. [8] gives a thorough description, with photographs, of the apparatus used.

Coolant was pumped into the heat exchangers at the same time as the downwards motion of the cell began. Pulling speeds in the range $0.1\text{--}10 \mu\text{m s}^{-1}$ were used. During the initial part of the experiment, a solid eutectic and mushy layer grew upwards from the bottom heat exchanger. The mushy layer eventually reached a steady-state height, which was measured and recorded. After several hours, the solution became depleted of ammonium chloride and the height of the mushy layer decreased. Thermistors embedded in the sides of the cell measured the temperature profile throughout the course of the experiment. In some experiments, an additional thermistor was used to measure the temperature profile in the centre of the cell, which was less affected by heat transfer through the sides of the cell.

Experiments with ammonium chloride were carried out using two different temperature gradients: 1.52°C/mm (achieved by maintaining the lower heat exchanger at $T_B = -35^\circ\text{C}$ and the upper at $T_L = +40^\circ\text{C}$, with a separation of $L = 4.95$ cm) and 0.69°C/mm ($T_B = -35^\circ\text{C}$, $T_L = 0^\circ\text{C}$, $L = 8.00$ cm). The error in each measurement of L is ± 0.05 cm.

3. Results

Figs. 2(a) and (c) summarise the results from temperature gradients 1.52 and 0.69°C/mm , respectively. Four different modes of solidification were observed, depending on the initial concentration and pulling speed used. The results obtained by Peppin et al. [9] using a temperature gradient of 0.92°C/mm have been reproduced in Fig. 2(b) for comparison.

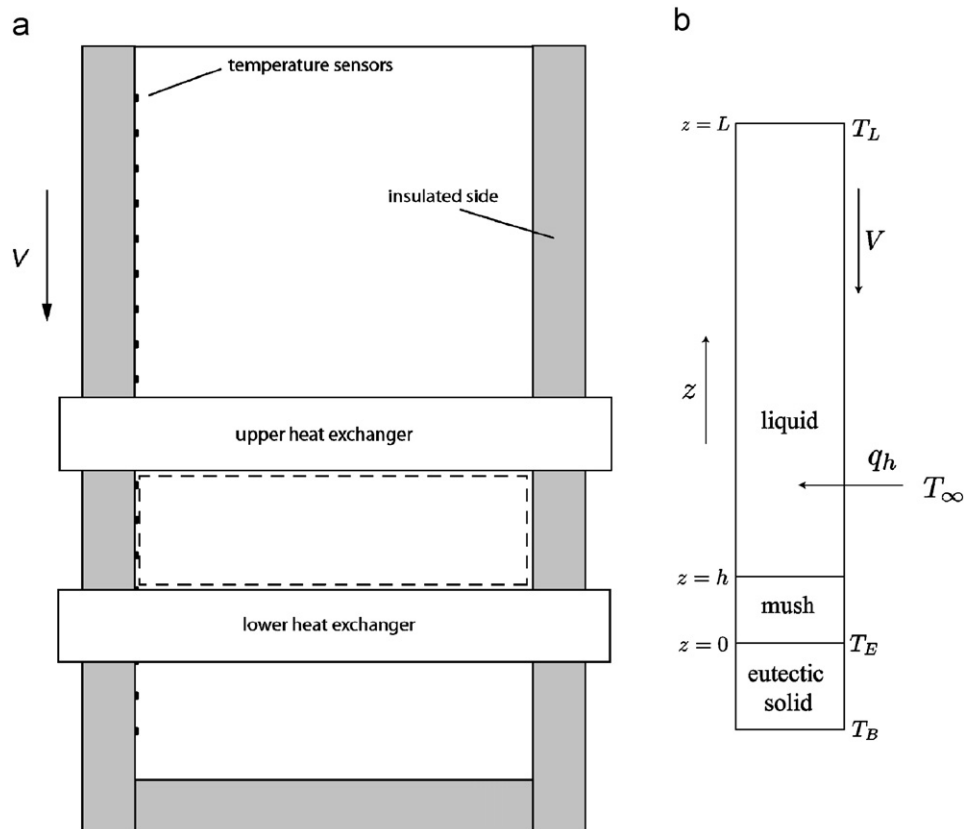


Fig. 1. (a) A schematic showing the experimental cell and heat exchangers. During the experiment, the cell is translated downwards between the heat exchangers at constant speed V by a screw mechanism driven by a stepper motor. Temperature sensors attached to the inside edge of the cell measure the temperature profile throughout the solidification experiment. The region between the heat exchangers, surrounded by a dashed line, is the computational domain, shown in (b). (b) A schematic of the computational domain as viewed from the side, showing the heat flux q_h into the cell from the air outside it. In the experiments at the high temperature gradient, in which the top heat exchanger is heated above room temperature, q_h will be negative for the upper part of the computational domain. We take $z = 0$ to be the position of the top of the eutectic. Because the eutectic does not grow very high above the bottom heat exchanger, the position of the top heat exchanger is approximately $z = L$. In steady-state, the top of the mushy layer is at $z = h$.

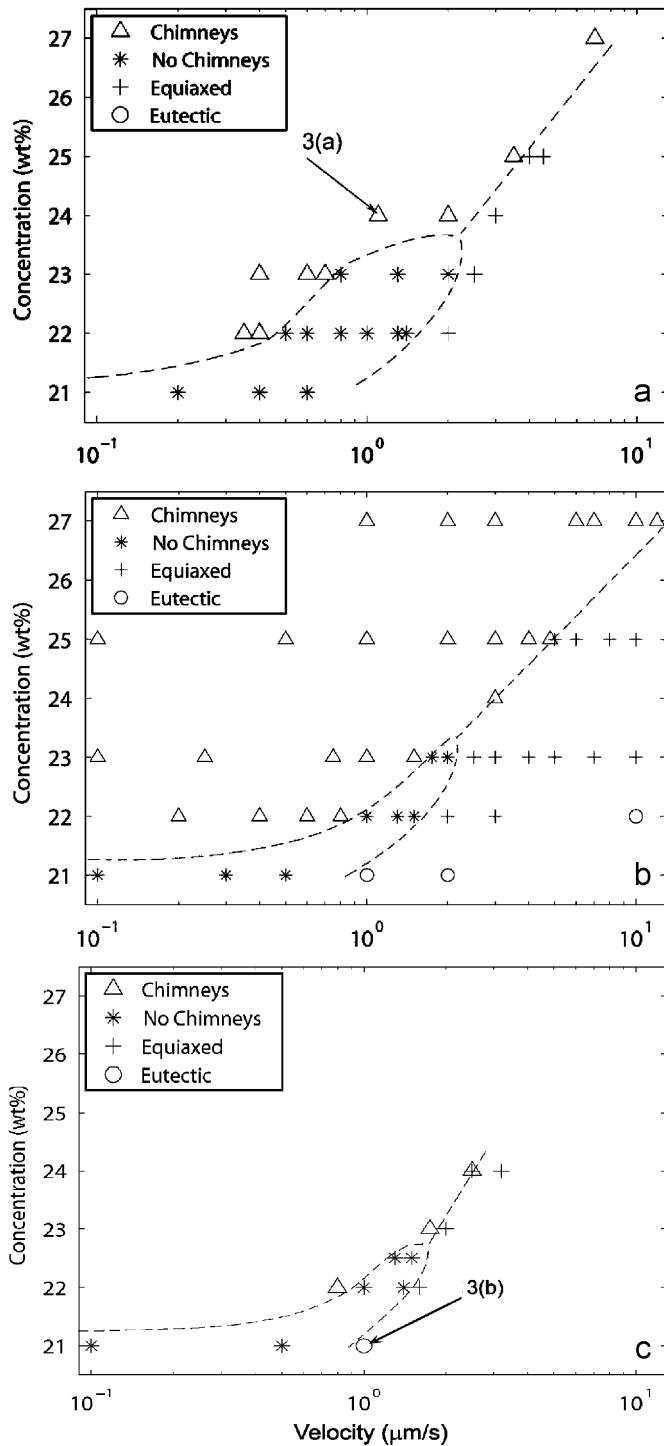


Fig. 2. Regime diagrams representing the different modes of solidification of ammonium chloride: (a) at high temperature gradient: $1.52\text{ }^{\circ}\text{C}/\text{mm}$, (b) at medium temperature gradient: $0.92\text{ }^{\circ}\text{C}/\text{mm}$ and (c) at low temperature gradient: $0.69\text{ }^{\circ}\text{C}/\text{mm}$. The points labelled 3(a) and (b) correspond to conditions at which the photographs in Figs. 3(a) and (b) were taken. The dashed curves have been hand-drawn to separate the different regimes.

At low pulling speeds and high initial concentrations, convection in the mushy layer causes chimneys to form. During growth of the mushy layer, vigorous convection is observed, with plumes rising from the mush. Some of these plumes quickly die out, whilst others become stronger and chimneys can be seen forming beneath them. A steady-state mushy layer with chimneys is shown in Fig. 3(a). Mushy layers with fewer, weaker chimneys are

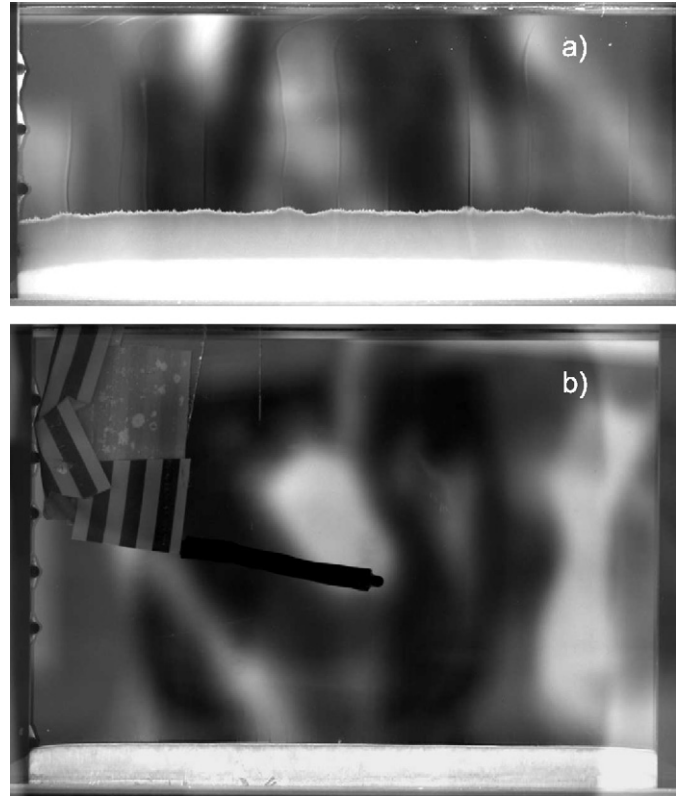


Fig. 3. (a) A steady-state mushy layer with chimneys, which was formed from 24 wt% aqueous NH_4Cl solution translated at $1.1\text{ }\mu\text{m s}^{-1}$ through a temperature gradient of $1.52\text{ }^{\circ}\text{C}/\text{mm}$; (b) 21% aqueous NH_4Cl solution forms a solid eutectic but no mushy layer when translated at $1\text{ }\mu\text{m s}^{-1}$ through a gradient of $0.69\text{ }^{\circ}\text{C}/\text{mm}$. The thermistor used to measure the temperature in the centre of the cell is also visible.

formed under conditions close to the chimney/no-chimney and chimney/equiaxed boundaries on the regime diagram.

As the mushy layer grows, solute is taken up in the dendrites, causing a decrease in concentration of the liquid just ahead of the solidification front and hence a depression of the local freezing temperature. The difference between the measured temperature at the mush–liquid interface and the freezing temperature of the original solution (the undercooling) is plotted in Fig. 4. At high pulling speeds, the undercooling is sufficient for crystals of ammonium chloride to nucleate in the region just above the interface. These secondary crystals, along with pieces of dendrite ejected from the mushy layer by convection currents, fall back into the mush, causing it to collapse and give way to a layer of equiaxed crystals. If the velocity is increased still further, the mush disappears altogether, leaving behind only the solid eutectic, as observed in Fig. 3(b).

For low concentrations, it was possible to grow a mushy layer without the presence of either chimneys or equiaxed growth. This is of interest because the result is a solid which is free from both freckles and grain boundaries. As is clear from the regime diagrams in Fig. 2, raising the temperature gradient increases the range of conditions that give rise to this mode of solidification. Whilst the boundary between the no-chimney and equiaxed regions appears to be relatively unmoved by an increase in temperature gradient, the chimney/no-chimney boundary is significantly shifted to lower velocity. Lowering the temperature gradient has the opposite effect, narrowing the width of the no-chimney region to the extent that it could not be observed at all at $C_0 = 23\text{ wt}\%$.

When solidifying 24 wt% NH_4Cl at the lower temperature gradient we observed another regime in which chimneys and

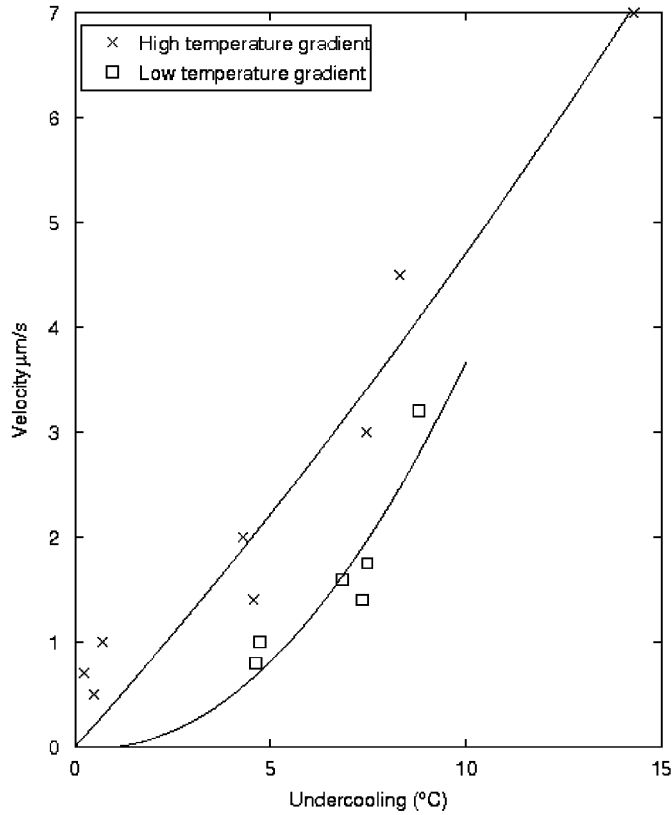


Fig. 4. Undercooling as measured at the mush–liquid interface using various pulling speeds at the high and low temperature gradients, with second-order polynomial fits of the form $V = G_1[T_L(C_0) - T_h] + G_2[T_L(C_0) - T_h]^2$. At the high temperature gradient $G_1 = 4.2 \times 10^{-7} \text{ m s}^{-1}/^\circ\text{C}$ and $G_2 = 5.4 \times 10^{-9} \text{ m s}^{-1}/^\circ\text{C}^2$, whilst at the low temperature gradient $G_1 = -4.2 \times 10^{-8} \text{ m s}^{-1}/^\circ\text{C}$ and $G_2 = 4.1 \times 10^{-8} \text{ m s}^{-1}/^\circ\text{C}^2$.

equiaxed growth co-exist in steady-state. This is in contrast to experiments performed at the higher temperature gradients, in which the steady-state mode of solidification could always be clearly identified as being in either the chimney or the equiaxed regime. The low temperature gradient produces this mixed regime at 24 wt% because the temperature profile is such that the whole of the liquid region between the heat exchangers is below the liquidus temperature, which promotes secondary nucleation above the mush–liquid interface. In fact many of the experiments performed at the low temperature gradient showed some secondary nucleation during growth.

The measured heights of the mushy layers at each concentration and velocity were compared with two sets of predictions of the heights, one of which was obtained by using the shooting method to solve the governing equations numerically, and the other by solving analytically the approximate model developed in Section 4. The matching of the predictions to the experimental data is discussed in Section 5. In general, the steady-state height of the mushy layer is decreased by increasing the temperature gradient.

4. Mathematical modelling

In this section we consider the equations governing temperature in the mush and melt regions and discuss how to solve them, first numerically and then by making approximations that allow us to find a useful analytical solution. We assume that there is no convection in the mush, so that this analysis applies to mushy

layers without chimneys. A schematic diagram of the computational region is shown in Fig. 1(b).

Heat transfer through the walls of the cell is modelled using Newton's law of cooling [10]:

$$\frac{dq_h}{dz} = b(T - T_\infty), \quad (2)$$

where q_h is the heat flux through the sides of the cell, T_∞ is the temperature of the air outside the cell and the heat transfer coefficient $b = 1600 \text{ J m}^{-3} \text{ s}^{-1} \text{ K}^{-1}$ has been determined experimentally by Peppin et al. [8]. Balancing this term against heat transfer by motion of the fluid and by diffusion gives

$$c_l V \frac{dT}{dz} + \frac{d}{dz} k_l \frac{dT}{dz} = b(T - T_\infty) \quad (3)$$

as the expression for conservation of energy in the liquid, where c_l and k_l are the effective volumetric heat capacity and thermal conductivity of the cell plus solution [8]. Eq. (3) is a linear, second-order, ordinary differential equation with constant coefficients, which has solutions proportional to exponential functions of z . Specifically we solve this equation subject to the boundary conditions $T(h) = T_h$ and $T(L) = T_L$, where T_h and T_L are the temperatures of the mush–liquid interface and upper heat exchanger, respectively, to find

$$T(z) = T_\infty + (T_h - T_\infty)f_1(z) + (T_L - T_\infty)f_2(z), \quad (4)$$

as the steady-state temperature profile in the liquid, where

$$f_1(z) = \frac{e^{r_1(z-L)} - e^{r_2(z-L)}}{e^{r_1(h-L)} - e^{r_2(h-L)}}, \quad (5)$$

$$f_2(z) = \frac{e^{r_1(z-h)} - e^{r_2(z-h)}}{e^{r_1(L-h)} - e^{r_2(L-h)}} \quad (6)$$

and $r_{1,2} = -c_l V / 2k_l \pm \frac{1}{2}(c_l^2 V^2 / k_l^2 + 4b/k_l)^{1/2}$.

In the mushy layer, the heat of solidification must also be considered, so that the expression for the conservation of energy in the mush is

$$-c_l V \frac{dT}{dz} = \frac{d}{dz} k_e \frac{dT}{dz} - \zeta \mathcal{L}_s V \frac{d\phi}{dz} - b(T - T_\infty), \quad (7)$$

where ζ is the fraction of the cross-sectional area of the Hele–Shaw cell occupied by solution, k_e is the effective thermal conductivity of the mush, \mathcal{L}_s is the latent heat of solidification and ϕ is the solid fraction of the mush. The terms in Eq. (7) represent, from left to right, advection of heat by downwards motion of the cell, thermal diffusion, the heat of solidification and the heat transfer through the sides of the cell.

By coupling this equation with an expression for the local conservation of solute in the mush,

$$(1 - \phi) \frac{dC}{dz} = (C - C_s) \frac{d\phi}{dz}, \quad 0 \leq z \leq h, \quad (8)$$

where C_s is the concentration of solute in the solid dendrites and diffusion of solute has been neglected, and using the liquidus relation

$$C_L(T) = [T(z) - T_E] / \Gamma + C_E, \quad (9)$$

where T_E is the eutectic temperature and Γ is the slope of the liquidus, Peppin et al. [9] derived a nonlinear equation for temperature in the mush:

$$\frac{d}{dz} k_e \frac{dT}{dz} = - \left(c_l V + \frac{\zeta \mathcal{L}_s V \Gamma C_0}{T^2} \right) \frac{dT}{dz} + b(T - T_\infty). \quad (10)$$

This was solved numerically using the shooting method, in which initial values of $dT/dz|_0$ and h are guessed and Eq. (10) is solved numerically for $T(h)$ and $dT/dz|_{h-}$. New values of $dT/dz|_0$ and h are then estimated using Newton's method, and the procedure is repeated until the values of T and dT/dz at $z = h$ match those

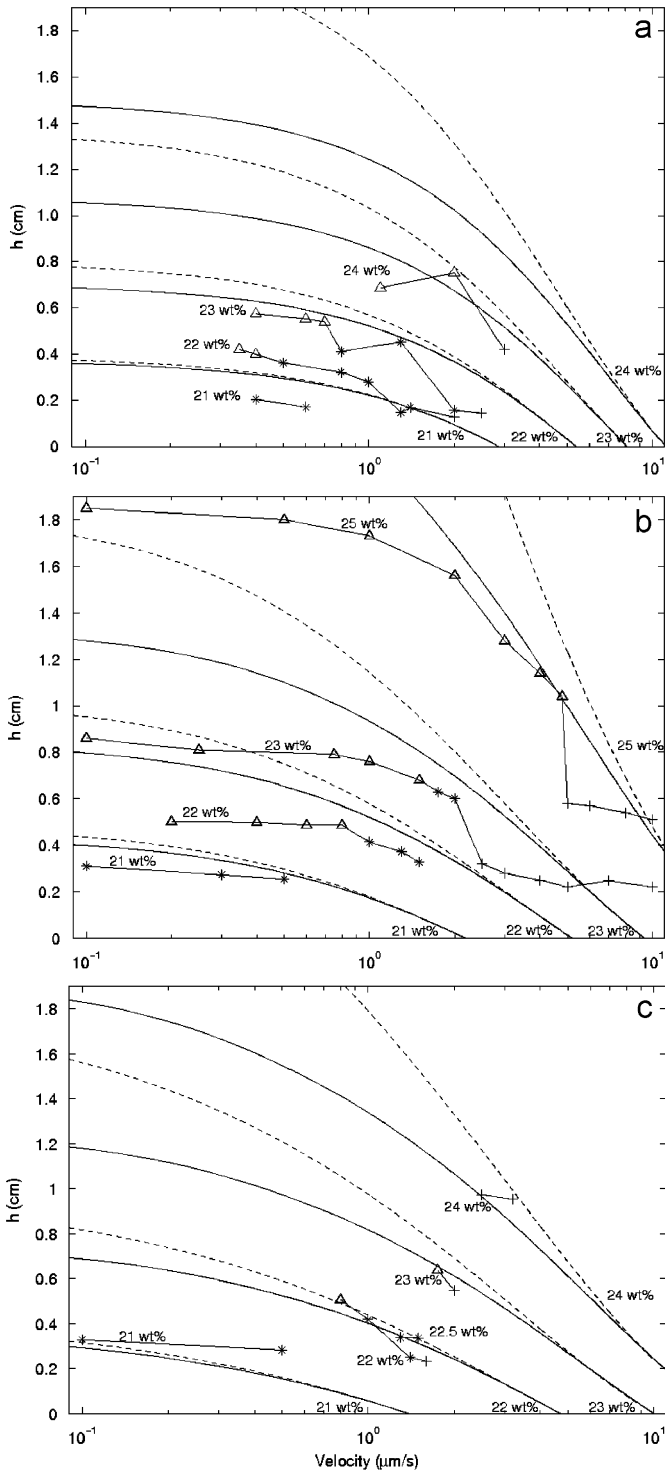


Fig. 5. Steady-state heights of the mushy layers grown using ammonium chloride along with numerical and analytical predictions: (a) at high temperature gradient: $1.52\text{ }^{\circ}\text{C}/\text{mm}$; (b) at medium temperature gradient: $0.92\text{ }^{\circ}\text{C}/\text{mm}$; (c) at low temperature gradient: $0.69\text{ }^{\circ}\text{C}/\text{mm}$. The smooth solid and dashed lines represent numerical and analytical solutions, respectively, for each concentration. The experimental data are plotted using the symbols defined in Fig. 2, with solid lines connecting points of the same concentration.

given by the solution for the liquid region (4). Using this method, Peppin et al. made predictions of the heights of the mushy layers which were a reasonably good match to experimental data, particularly at high pulling speeds, as reproduced in Fig. 5(b). We have applied the same numerical method to predict the values of

h at the high and low temperature gradients, with better matching to experimental data when the temperature gradient is lower (Figs. 5(a) and (c)).

Here we obtain an approximate analytical solution for the temperature profile, which will be used to predict values of h to compare directly with numerical and experimental data. An analytic, albeit approximate, solution is extremely valuable because it makes the dependence of T and h on each parameter explicit, and so we can predict how they will respond to changes in the parameters without having to run a numerical simulation for each new value. Also, although the approximate solutions will not hold under all conditions, they may still provide valuable physical insight into the process of solidification.

The first approximation we make is to assume that the solid fraction ϕ decreases linearly with z , such that

$$\phi = \phi_E(1 - z/h). \quad (11)$$

The actual relation between ϕ and z is unknown. This approach of prescribing a functional form to a dependent field variable can lead to good predictions of integral properties of the system, such as the depth of the mushy layer and its mean solid fraction. Indeed, the authors of Ref. [11] make the assumption that ϕ is constant throughout the mushy layer to derive a model which gives good agreement with experimental results. Better agreement is achieved in Ref. [12], which discusses numerical modelling of the mushy layer in which ϕ is allowed to vary with z , but the improvement is small. We make the first-order approximation of linear $\phi(z)$ to satisfy the condition for marginal equilibrium, $\phi(h) = 0$, and match the result found in Ref. [12] that ϕ is small throughout the layer and decreases with increasing z .

The constant ϕ_E is found by substituting for ϕ in the global conservation of solute

$$\int_0^h \phi C_S + (1 - \phi)C_L(T) dz = C_0 h, \quad (12)$$

where C_S is the concentration of solute in the solid dendrites and $C_L(T)$ is the concentration in the liquid. The solution is assumed to be in local equilibrium, so that the liquidus relation (9) always holds. In order to obtain an expression for ϕ_E which has a simple linear dependence on h , we assume a linear temperature profile in the mush,

$$T = T_E + (T_h - T_E)z/h, \quad (13)$$

where T_h is the temperature at the mush–liquid interface as given by the undercooling relation

$$V = G_1[T_L(C_0) - T_h] + G_2[T_L(C_0) - T_h]^2, \quad (14)$$

with constants G_1 and G_2 determined by fitting a second-order polynomial to empirical data (Fig. 4). Experimental measurements of the temperature profile show that this is a reasonable approximation. After substituting Eq. (13) into Eq. (12), we evaluate the integral and rearrange to find

$$\phi_E = \frac{6\Gamma(C_0 - C_E) - 3(T_h - T_E)}{3\Gamma(C_S - C_E) - (T_h - T_E)}. \quad (15)$$

Now that ϕ_E is known, we make further approximations to Eq. (7) by neglecting the term describing the translation of the cell, $c_l V dT/dz$, because it is significantly smaller than the other terms. We also make the assumption that no heat is lost through the sides of the cell from the mush, so that $b = 0$ in Eq. (7), although we will account for heat losses in the melt. By comparing the relative sizes of the neglected terms with those that are retained, which we do in Appendix A, we can justify making these approximations when the Péclet number

$$Pe = \frac{c_l V h}{k_e} \quad (16)$$

is small and the Stefan number

$$\mathcal{S} = \frac{\mathcal{L}_s}{c_l(T_L(C_0) - T_E)} \quad (17)$$

is large.

The resulting equation

$$k_e \frac{d^2 T}{dz^2} = -\frac{\zeta \mathcal{L}_s V \phi_E}{h} \quad (18)$$

can be readily solved for T , subject to the boundary conditions [13]

$$T(0) = T_E, \quad \left. \frac{dT}{dz} \right|_{h^-} = \left. \frac{dT}{dz} \right|_{h^+}, \quad (19)$$

where $dT/dz|_{h^+}$ is found by differentiating Eq. (4). The approximate solution is

$$T(z) = T_E + [(T_h - T_\infty)f'_1(h) + (T_L - T_\infty)f'_2(h)]z + \frac{\zeta \mathcal{L}_s V \phi_E}{k_e} z - \frac{\zeta \mathcal{L}_s V \phi_E}{2k_e h} z^2, \quad (20)$$

where we evaluate $f'_1(h)$ and $f'_2(h)$ using the assumption $h \ll L$, such that they are both independent of h and given by

$$f'_1(h) \approx \frac{r_1 e^{-r_1 L} - r_2 e^{-r_2 L}}{e^{-r_1 L} - e^{-r_2 L}} \quad \text{and} \quad (21)$$

$$f'_2(h) \approx \frac{r_1 - r_2}{e^{r_1 L} - e^{r_2 L}}. \quad (22)$$

In our experiments, L was usually at least five times h .

We now use this expression for T to make predictions of the heights of the mushy layers produced using various initial concentrations and pulling speeds. We set $T(h) = T_h$, and rearrange the result into the analytical expression for the height of the mushy layer

$$h = \frac{T_h - T_E}{\frac{\zeta \mathcal{L}_s V \phi_E}{2k_e} + (T_h - T_\infty)f'_1(h) + (T_L - T_\infty)f'_2(h)}, \quad (23)$$

into which we can substitute for ϕ_E using Eq. (15).

Predictions of h made using this expression are compared with numerical and experimental data at each temperature gradient in Fig. 5. The approximate analytical model gives predictions of h that are in very good agreement with the numerical predictions, particularly for small h or large V .

5. Discussion

Convection in the mushy layer is responsible for the formation of chimneys. As the Rayleigh number governing convection in the mush is linearly dependent on C_0 , high initial concentrations of solute in the solidifying fluid usually give rise to chimneys. If the pulling velocity is increased sufficiently, however, then the undercooling just above the mush–liquid interface becomes sufficiently large to cause secondary nucleation and the chimney regime gives way to a regime of equiaxed growth (Fig. 2). For aqueous ammonium chloride solutions of initial concentration of or above 24 wt% at high temperature gradient, or 23 wt% at low temperature gradient, it was impossible to grow a defect-free solid.

At low C_0 , however, a regime exists where neither the convection in the mushy layer nor the undercooling above it are sufficiently large to cause defects to form in the solid. This regime can be enlarged by increasing the temperature gradient, because this has the effect of decreasing the height of the mushy layer, thus decreasing the Rayleigh number and inhibiting convection.

Predictions of h made using the approximate solution match numerical predictions very closely when h is small and V is large,

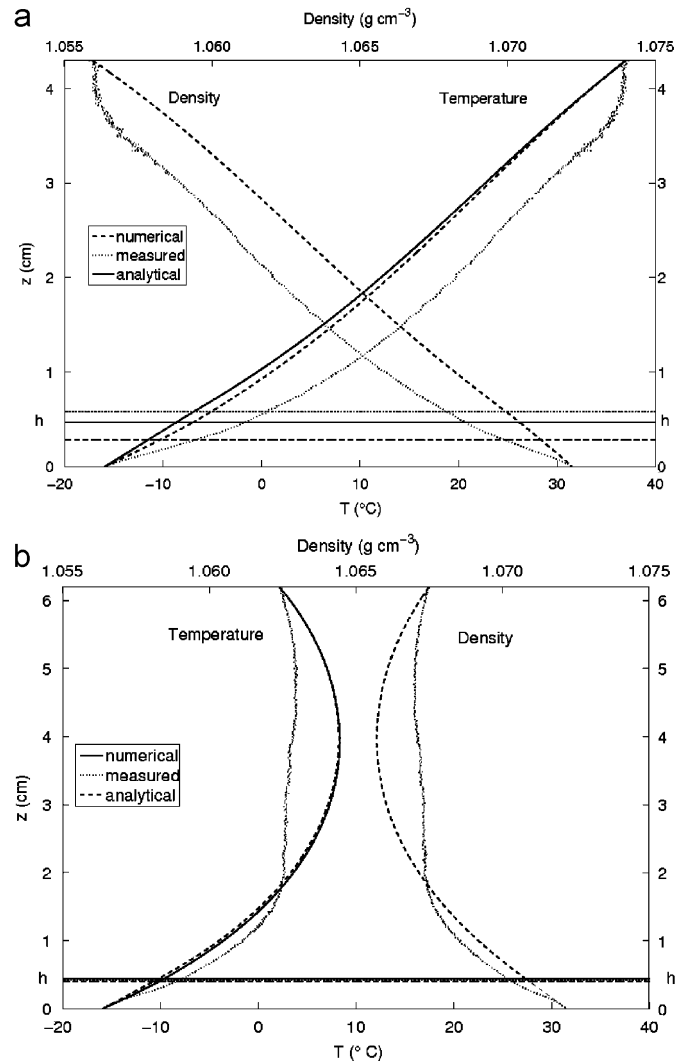


Fig. 6. Temperature and density profiles during steady-state solidification of 22 wt% NH_4Cl [$T_L(C_0) = -4.63^\circ\text{C}$] at $V = 1 \mu\text{m s}^{-1}$: (a) at high temperature gradient, 1.52°C/mm , where the roughness of the experimental curve close to the top of the cell is due to penetration from convection driven by an unstable thermal distribution in the fluid above the top heat exchanger and (b) at low temperature gradient, 0.69°C/mm . Density has been calculated from temperature using a relation derived from data from Ref. [14]. The horizontal lines represent the measured and predicted values of h .

as expected for the reasons given in Appendix A. Both predictions match the experimental data very closely at low temperature gradient, although they are much less accurate when the gradient is high (Fig. 5). At high temperature gradient, moreover, the temperature profile across the cell (Fig. 6(a)), whilst having a similar shape to the measured profile, is predicted to be up to 10°C lower than the measured values. This suggests that the theoretical model is not a good description of the system when the temperature gradient is high.

At low temperature gradient the temperature across the middle part of the cell is almost constant, which is very different from the predicted profile (Fig. 6(b)). This is because the model treats convection in the melt as negligible, whereas in fact in the upper part of the cell the static density profile in the fluid increases with height. The convection resulting from this unstable distribution penetrates into the rest of the fluid (as discussed in Ref. [15]), causing a significant redistribution of heat. In the lower, non-conducting part of the cell, however, the matching between predicted and measured profiles is good, suggesting that our

theory is a good model for solidification in the absence of convection.

6. Conclusion

There are two important conclusions to be drawn from this work.

Firstly, experiments with ammonium chloride have shown that the range of conditions which give rise to defect-free solidification of a binary alloy can be expanded by an increase in temperature gradient.

Secondly, we have succeeded in approximating the governing equations of heat transfer in the mushy layer in such a way as to allow an analytical solution to be found. We have demonstrated that this approximate solution gives predictions of the height of the mushy layer which tend to the numerical solutions as the height of the mush becomes small, and which are also a close match to the experimental results at low temperature gradient. Consideration of the relative sizes of the terms in the original equations has allowed us to give an indication of the range of parameters for which our approximate model is valid.

Acknowledgements

We thank M.A. Hallworth and D. Page-Croft for technical assistance with the experiments, and S.S.L. Peppin, G. Amberg and R.C. Kerr for their helpful comments on an earlier draft of the manuscript. We also thank S.S.L. Peppin for discussions concerning the experiments. The research of S.H.W. was supported by an EPSRC Summer Student Bursary Scheme and of H.E.H. by a Royal Society Wolfson Merit Award.

Appendix A. Justification of approximations

In order to quantify the range of conditions under which the analytical approximation applies, it is necessary to re-examine Eq. (7) and consider the relative size of each term. We use characteristic scales of length and temperature to approximate each term such that

$$c_l V \frac{dT}{dz} \sim c_l V \frac{(T_L(C_0) - T_E)}{h}, \quad (\text{A.1})$$

$$\frac{d}{dz} k_e \frac{dT}{dz} \sim k_e \frac{T_L(C_0) - T_E}{h^2}, \quad (\text{A.2})$$

$$\zeta \mathcal{L}_s V \frac{d\phi}{dz} \sim \zeta \mathcal{L}_s V \frac{\phi_E}{h}, \quad (\text{A.3})$$

$$b(T - T_\infty) \sim b(T_L(C_0) - T_\infty) \quad (\text{A.4})$$

and set $\phi_E = 1$ for convenience. A term can be neglected if its characteristic size is much smaller than the terms to be retained.

Thus the term $c_l V dT/dz$ can be neglected provided that it is small compared to the diffusion term, which occurs if the Péclet number

$$Pe = \frac{c_l V h}{k_e} \ll 1. \quad (\text{A.5})$$

We also require that this term is small compared to the solidification term, i.e. that the Stefan number

$$\mathcal{S} = \frac{\mathcal{L}_s}{c_l(T_L(C_0) - T_E)} \gg 1. \quad (\text{A.6})$$

These two conditions are related in that, in the limiting case of very large Stefan number considered in Ref. [13], $h \propto \ln(1 + 1/\mathcal{S})$, which reduces via a Taylor approximation to $h \propto \mathcal{S}^{-1}$. Thus, satisfaction of condition (A.6) implies that h is small so that condition (A.5) is also satisfied. In the case of solidification of NH_4Cl in the Hele–Shaw cell, condition (A.6) is satisfied for $C_0 \ll 37$ wt%, which is true for all the experiments carried out.

Comparing the heat loss term $b(T - T_\infty)$ to the diffusion term and making the approximation that, within one order of magnitude, $T_L(C_0) - T_\infty \sim T_L(C_0) - T_E$, we derive the condition that $h^2 \ll k_e/b$, which is easily met in all of our experiments. We thus compare the heat loss term to the solidification term to derive the condition

$$h \ll \frac{\zeta \mathcal{L}_s V}{b[T_E - T_\infty + \Gamma(C_0 - C_E)]}, \quad (\text{A.7})$$

which is the limiting condition on the validity of the approximation, with the analytical model fitting the numerical data better at large V and small h .

References

- [1] B.H. Kear, *Sci. Am.* 255 (1986) 159.
- [2] M.G. Worster, *J. Fluid Mech.* 237 (1992) 649.
- [3] M.G. Worster, *Solidification of fluids*, in: G.K. Batchelor, H.K. Moffatt, M.G. Worster (Eds.), *Perspectives in Fluid Dynamics*, Cambridge University Press, UK, 2000, pp. 393–446.
- [4] J.S. Wettlaufer, M.G. Worster, H.E. Huppert, *J. Fluid Mech.* 344 (1997) 291.
- [5] S.M. Copley, A.F. Giamei, S.M. Johnson, M.M. Hornbecker, *Metall. Trans.* 1 (1970) 2193.
- [6] F. Chen, C.F. Chen, *J. Fluid Mech.* 227 (1991) 567.
- [7] S. Tait, C. Jaupart, *J. Geophys. Res.* 97 (1992) 6735.
- [8] S.S.L. Peppin, P. Aussillous, H.E. Huppert, M.G. Worster, *J. Fluid Mech.* 570 (2007) 69.
- [9] S.S.L. Peppin, H.E. Huppert, M.G. Worster, *J. Fluid Mech.* 599 (2008) 465.
- [10] F.P. Incropera, D.P. DeWitt, *Fundamentals of Heat and Mass Transfer*, fourth ed., Wiley, New York, 1996, pp. 113–114.
- [11] H.E. Huppert, M.G. Worster, *Nature* 314 (1985) 25.
- [12] M.G. Worster, *J. Fluid Mech.* 167 (1986) 481.
- [13] M.G. Worster, *J. Fluid Mech.* 224 (1991) 335.
- [14] E.W. Washburn, *International critical tables: numerical data, physics, chemistry and technology*, New York, 1926.
- [15] J.S. Turner, *Buoyancy Effects in Fluids*, Cambridge University Press, UK, 1973, pp. 251–287.